PAPER • **OPEN ACCESS**

Dynamic Frictional Sliding Modes between Two Homogenous Interfaces

To cite this article: W Taj and D Coker 2018 *IOP Conf. Ser.: Mater. Sci. Eng.* **295** 012001

Dynamic Frictional Sliding Modes between Two Homogenous Interfaces

Taj W[2], Coker D[1]
[1]*Department of Aerospace Engineering, Middle East Technical University, 06800, Ankara, Turkey*
[2] *Department of Aerospace Engineering, Middle East Technical University, Ankara, Turkey*
[2] *TUBITAK-UZAY Space Technologies Research Institute, 06800, Ankara, Turkey*
coker@metu.edu.tr[1], waheedullah.taj@metu.edu.tr[2]

Abstract: Dynamic frictional sliding behaviour between two homogenous Homalite blocks is studied. The blocks are initially held together using a constant compressive stress. The sliding motion is initiated by impacting one of the blocks with an external object. The resulting sliding modes are inspected. Initiation of fretting is examined by studying the opening stresses in the interface.

Keywords: FEM, Dynamic friction, impact, crack

1. Introduction

Dynamic frictional sliding between two bodies is a fundamental problem encountered in many engineering and science problems in various scales such as fiber reinforced composite material failure, earthquake faults during rupture, machining processes and surface interactions of moving machinery.
The behavior of the frictional interface during sliding motion is of extreme importance as it could explain many important phenomena such as fretting, energy dissipation and fatigue failure of the surface. Previous studies have discovered many sliding modes such as crack-like mode, which resembles a shear crack, a train of pulses mode and a growing pulses mode [1-3]. In a crack-like sliding mode the speed at the crack tip rapidly grows to a moderate level and stays there until the end of the interface. On the other hand, train of pulses sliding mode consists of small but powerful pulses across the interface reaching relatively high speed. In this sliding mode, the pulses maintain a relatively constant peak velocity. Finally, in growing pulses sliding mode there is one leading pulse with extremely high speed followed by a large number of smaller pulses. The aforementioned sliding modes are seen in specific loading and impact velocity conditions, however the regions of transition between the modes has not yet been studied in detail.
In this study, we examine the internal stresses and openings in sliding bodies. Our model uses a rate- and state-dependent friction law developed by Ref. [4]. The model uses the same configuration as in Ref. [3]. The model simulates two thin Homalite blocks held together in space using a constant compressive stress. One of the blocks is then impacted on one side with an external object. The resulting interfacial shear and normal stresses, opening stresses in the material, sliding velocity distribution across the interface and coefficient of friction are then examined in detail.

2. Problem Formulation

2.1. Cohesive law

The finite element code has two constitutive relations consisting of the bulk material constitutive law relating the stresses and strains in the material along with the cohesive law that gives the relation along the interface.

$$\dot{T}_n = -C_n \Delta \dot{u}_n \,, \quad \dot{T}_s = C_s[\Delta \dot{u}_s - sgn(T_s)\dot{q}_{slip} \tag{1}$$

where slip $\dot{q}_{slip}$ is the sliding rate at the interface. The expression for the slip or sliding rate is the dependent relation shown below

$$\dot{q}_{slip} = \begin{cases} \dot{q}_0(\beta^m - 1) & for\ \beta > 1 \\ 0 & for\ \beta \leq 1 \end{cases} \tag{2}$$

Where β is defined as

$$\beta = \frac{|T_s|}{T_n g(\theta)} \tag{3}$$

The friction equations are then updated using a single step tangent modulus method for rate dependent solids [5].

The following equation is used to calculate the change in sliding (horizontal) velocity

$$\Delta u(t) = u_x^+ - u_x^- \tag{4}$$

where u_x is the displacement in the *X*-direction of an interfacial point such that u_x^+ belongs to the point in the upper plate and u_x^- belongs to the corresponding point in the lower plate. The relative slip velocity can be found using a derivative definition as

$$\dot{q}_{slip} = \frac{\Delta u(t+\Delta t) - \Delta u(t)}{\Delta t} \tag{5}$$

2.2. Rate- and state-dependent friction law

The rate- and state-dependent friction law proposed by Ref. [4] and used by Ref. [3] has the following form

$$\mu(\theta_{ss}, \dot{u}_{slip}) = \mu_{ss} = \mu_d + (\mu_s - \mu_d) \exp\left(-\left(\frac{\dot{u}_{slip}}{V_1}\right)^p\right) \tag{6}$$

where μ_s and μ_d are coefficients of static and dynamic friction, and V_1, V_0, m and p are constants obtained from experiments. The values of these parameters are given in Table 1. This model of friction predicts that coefficient of friction decreases with slip velocity, as shown in Figure 1 (left). If there is no motion in the model initially, but then a finite slip velocity is applied, the model predicts that the coefficient of friction first rises to a maximum value, before decreasing to a value lower than before. If on the other hand, the velocity is suddenly decreased, the coefficient of friction first drops to a floor value before reaching a steady state higher than before. This behavior is seen in Figure 1 (right).

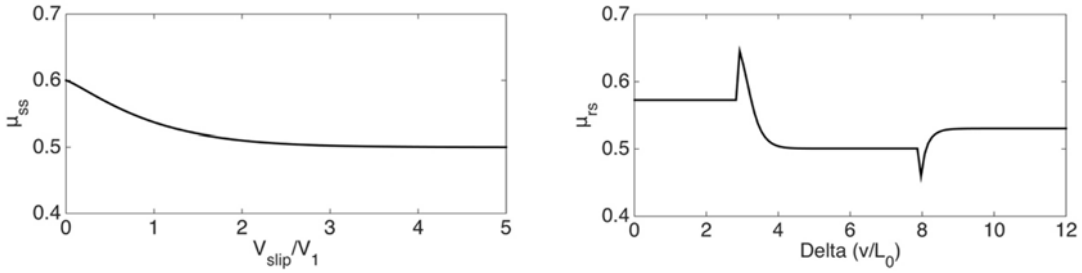

Figure 1. Coefficient of friction in steady state versus normalized velocity (left), and coefficient of friction versus delta with slip velocities: v_{slip} = 10 m/s for *delta* = 0 to *delta* = 3, v_{slip} = 100 m/s for *delta* = 3 to *delta* = 8 and v_{slip} = 30 m/s for *delta* = 80 to *delta* = 100 (right).

Table 1. Values of the parameters used in friction calculations in this study.

μ_s	μ_d	V_0 (μm/s)	V_1 (μm/s)	B	P	m	L_0 (μm)
0.6	0.5	100	26	1	1.2	5	20

2.3. Finite element model

The finite element model consists of two two dimensional blocks with dimensions of h = 75 mm and w = 200 mm each. The two blocks are pressed together with a uniform external loading of σ_0 until time t=0, at t=0 an impact velocity of $V(t)$ is given to the upper left side of the bottom block starting from X=0 up to Y=b=25mm. The dashed line in Figure 3 shows the cohesive interface between the two blocks. The X-Y coordinate system is defined such that X is parallel to the cohesive interface and Y is perpendicular to it. The origin of the coordinate system is selected as the left end of the cohesive interface. The mesh with rectangular elements used in finite element modelling is shown in Figure 4. A very fine uniform mesh was used at the left side of the model from X=0 to Y=80mm and from Y=0 to Y=±2mm. The mesh was then increased in coarseness starting from X=80mm to X=120mm at the left and Y=±2mm to Y=±20mm at the top. The rest of the mesh consisted of a uniform and relatively coarse mesh.

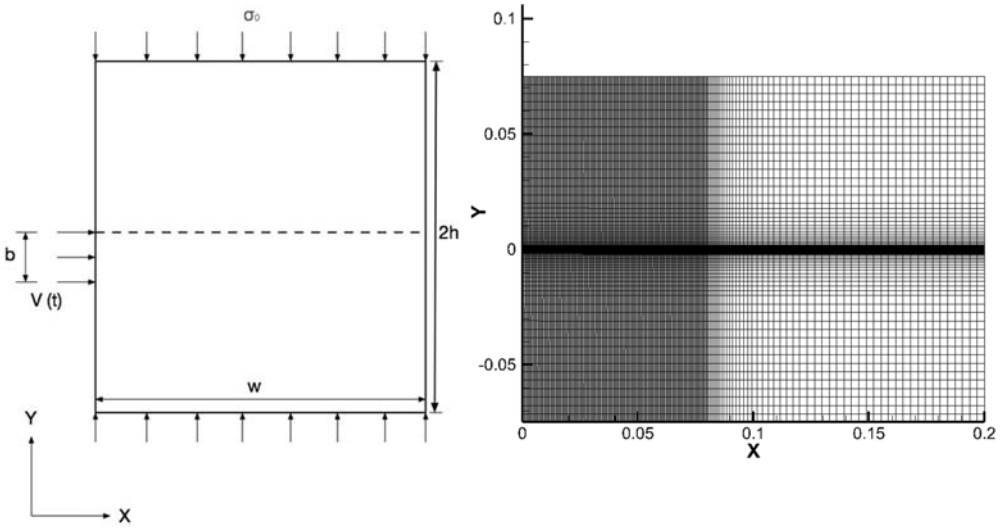

Figure 2. Finite element model (left) and finite element mesh (right).

The elastic properties of homalite used in this simulation are listed in Table 1.

Table 1. Elastic properties of Homalite used in the simulations.

E (GPa)	ν	ρ	c_l	c_s	c_R
5.3	0.35	1246	2201	1255	1170

Note that c_l, c_s, and c_R in Table 1 denote longitudinal wave speed, shear wave speed and Rayleigh wave speed of Homalite-100 respectively.

3. Results

Three different sliding modes were observed in the simulations. A crack-like mode, a train of pulses mode and a growing pulses mode. It has been observed that for a constant impact velocity of 10 m/s as compressive stress is increased the sliding mode transitions from crack-like to train of pulses to growing pulses mode.

3.1. Crack-like sliding mode

Figure 3 shows plots of sliding velocity and interfacial shear stress (left) and total slip displacement (right) vs. distance from the left side for the case σ_o = 5 MPa and V_{imp} = 10 m/s at time t = 34 μs. In this sliding mode sliding velocity suddenly jumps to a certain level, and then stays relatively constant until the end of the interface. Note that shear stress in the interface has progressed ahead of the sliding velocity. Shear stress builds up in the interface until it is enough to generate motion.
Figure 4 shows contour plots of maximum shear stress and normal stress in the horizontal direction, S_{XX}. The shape of the shear stress plot at X = 0.6 m closely resembles shear cracks, and hence the name of this sliding mode. S_{XX} is zero throughout the interface, except for the region of impact where it rises to very high levels, as is expected.
Figure 5 displays normal and shear stresses at the upper and lower surfaces of the interface and a close up of the interface. It is worth noting that S_{XX} is positive in the upper surface. This could lead to fretting and consequently fatigue failure of the interface. The close up of the interface suggests that there is no opening of the interface in this case. However there is an interpenetration. A small degree of interpenetration is allowed by the code to prevent numerical divergence.

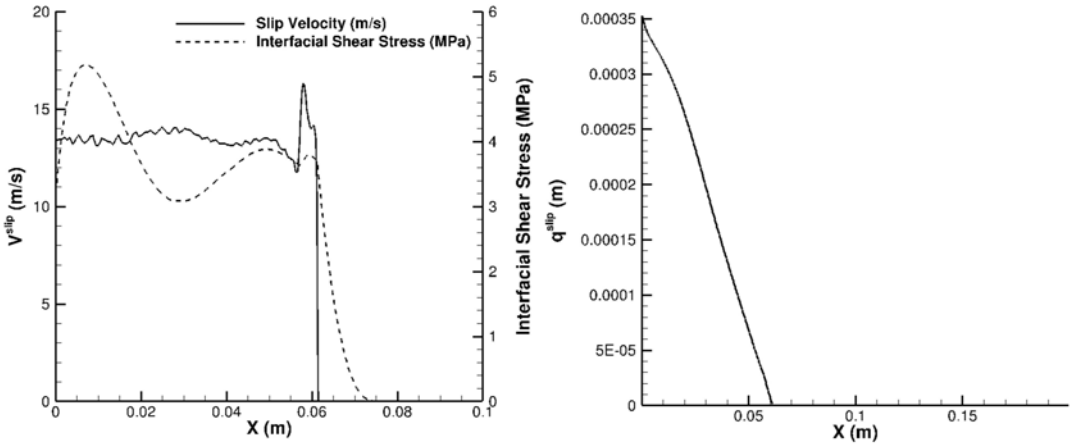

Figure 3. Sliding velocity and interfacial shear stress (left) and total slip displacement (right) vs. distance from the left side (t = 34 μs, σ_o = 5 MPa, V_{imp} = 10 m/s)

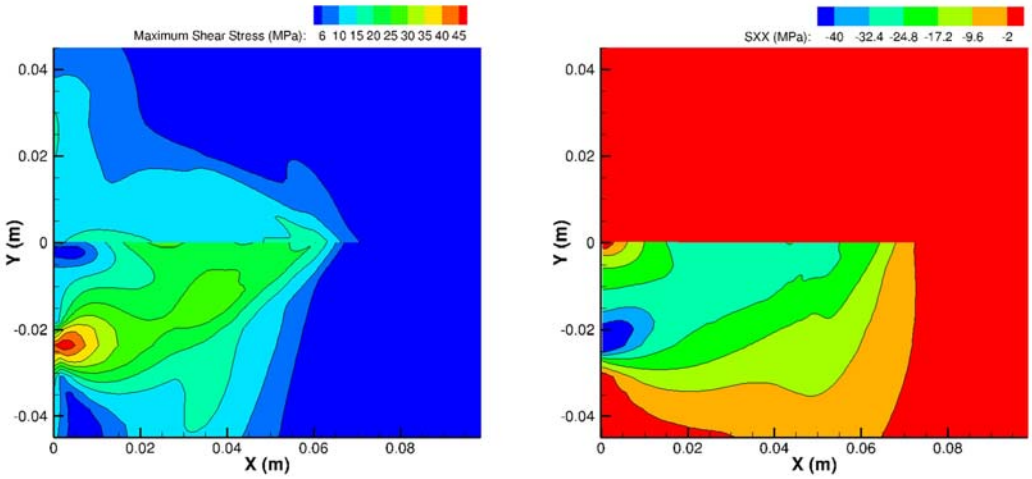

Figure 4. Contour plots of maximum shear stress (left) and horizontal normal stress, S_{XX} (right) throughout the specimen (t = 34 μs, σ_o = 5 MPa, V_{imp} = 10 m/s)

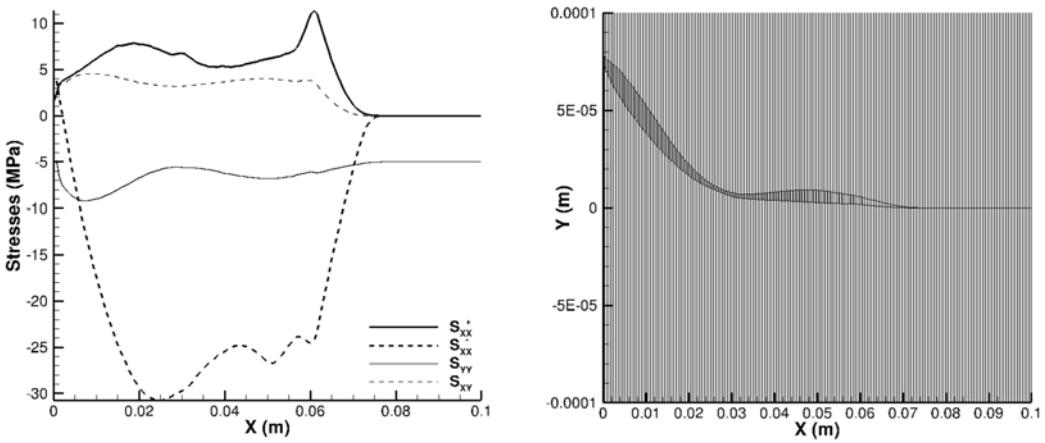

Figure 5. Plots of horizontal normal stress at the upper surface (S_{XX}^{+}), lower surface (S_{XX}^{-}), vertical normal stress (S_{YY}) and shear stress (S_{XY}) (left) and close-up of the mesh at the region of impact (right) (t = 34 μs, σ_o = 5 MPa, V_{imp} = 10 m/s)

3.2. Train of pulses sliding mode

Figure 6 shows plots of sliding velocity and interfacial shear stress (left) and total slip displacement (right) vs. distance from the left side for the case σ_o = 15 MPa and V_{imp} = 10 m/s at time t = 38 μs. In this sliding mode sliding velocity suddenly jumps to a moderately high level and then suddenly drops to zero. This pattern is repeated throughout the interface. Figure 6 (left) shows that shear stress in the interface builds up to relatively high levels before suddenly all the energy is released into a pulse. The plot of total displacement (Figure 6 (left)) has a stair-like shape which is a direct result of the velocity pulses in the interface.

Figure 7 plots contours of maximum shear stress and horizontal normal stress S_{XX} throughout the specimen. Notice that in this case the "crack tip" moves faster than the previous case. This is evident by the slope of the "crack tip" in the maximum shear stress plot.

Horizontal normal stress is again zero away from the region of impact, but close to region of impact it is positive in the upper surface and negative in the lower surface. This is further evident in the plot of Figure 8 (left). The stresses follow the pattern of the pulses just like interfacial shear stress. Figure 8

(right) is particularly interesting because it reveals that despite the heavier compressive loading there is an opening in the interface.

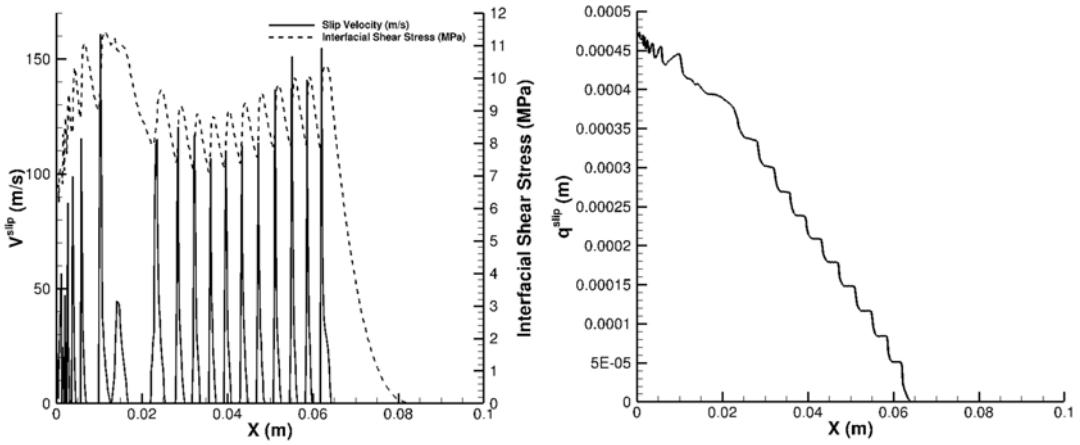

Figure 6. Sliding velocity and interfacial shear stress (left) and total slip displacement (right) vs. distance from the left side (t = 38 μs, σ_o = 15 MPa, V_{imp} = 10 m/s)

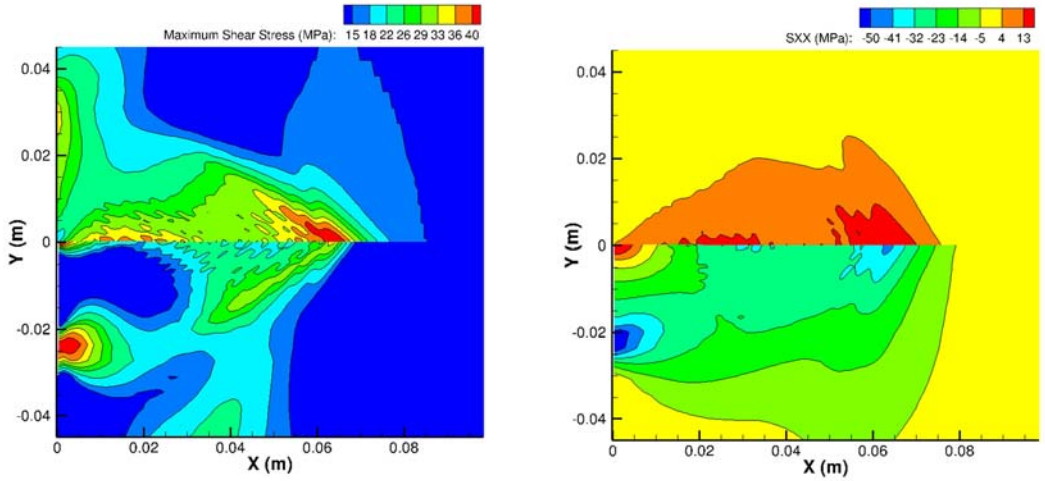

Figure 7. Contour plots of maximum shear stress (left) and horizontal normal stress, S_{XX} (right) throughout the specimen (t = 38 μs, σ_o = 15 MPa, V_{imp} = 10 m/s)

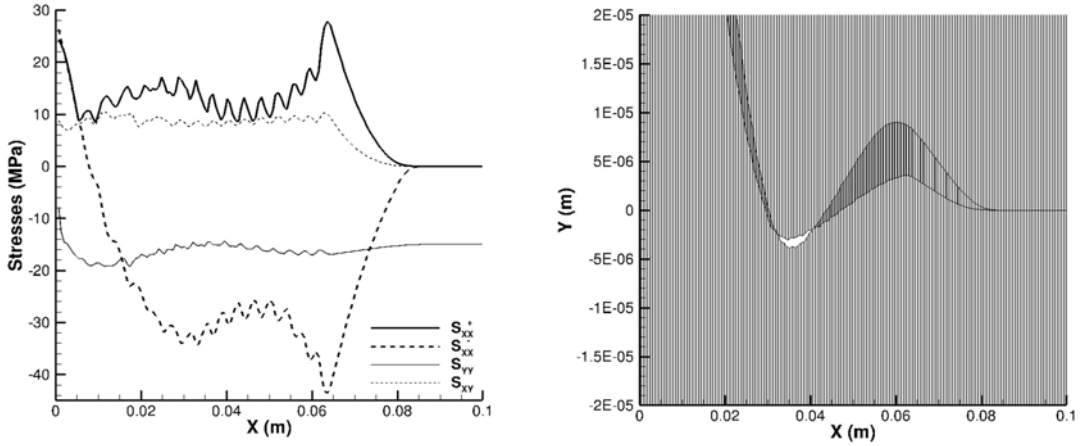

Figure 8. Plots of horizontal normal stress at the upper surface (S_{XX}^+), lower surface (S_{XX}^-), vertical normal stress (S_{YY}) and shear stress (S_{XY}) (left) and close-up of the mesh at the region of impact (right) (t = 38 μs, σ_o = 15 MPa, V_{imp} = 10 m/s)

3.3. Growing pulses sliding mode

We now look at the case where the compressive stress is increased to σ_o = 25 MPa, at the same impact speed of V_{imp} = 10 m/s. Figure 9 shows the sliding velocity and interfacial shear stress (left) and total slip displacement (right) vs. distance on the interface at time t = 20 μs. Multiple slip pulses with oscillating stresses corresponding to stick-slip motion are observed. At first sight this mode is similar to train of pulses sliding mode, however a closer look reveals the differences between the two cases. Although, pulses are observed in the sliding velocity profile, just like the previous sliding mode, unlike the previous mode the peak velocities of the pulses in this mode reach very high levels and the pulses are further apart and act as individual solitary pulses. Plot of total displacement is again stair-shaped, but the stairs are larger and less numerous as a direct consequence of the sliding velocity profile. Contour plot of maximum shear stress shown in Figure 10 (left) is even more inclined than the previous case meaning that the shear front is moving much faster. Plot of horizontal normal stress in Figure 10 shows traits very similar to the previous case, but in this case the stress level is lower. In this case the opening in the mesh vanishes.

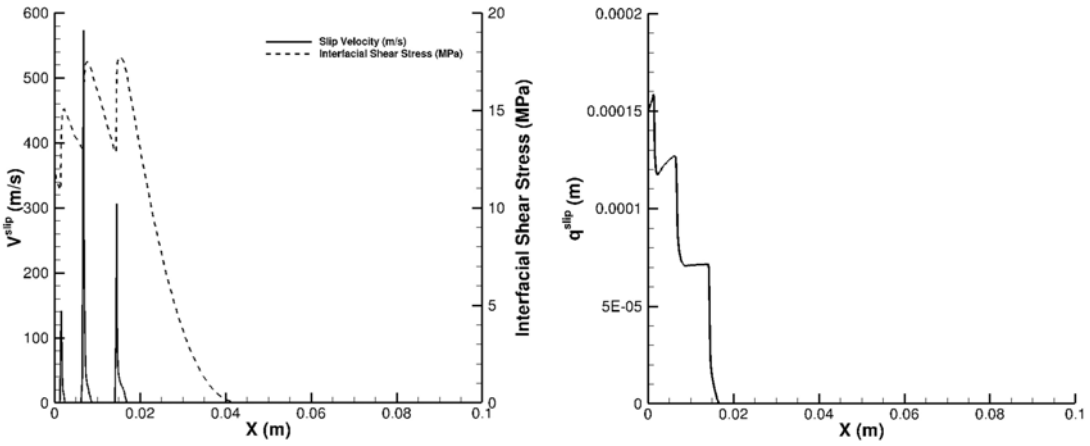

Figure 9. Sliding velocity and interfacial shear stress (left) and total slip displacement (right) vs. distance on the interface. (t = 20 μs, σ_o = 25 MPa, V_{imp} = 10 m/s)

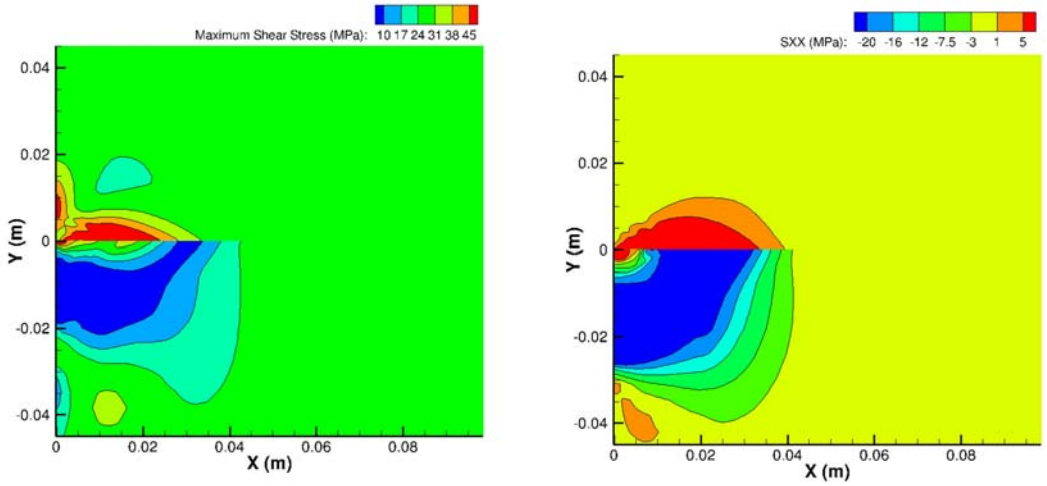

Figure 10. Contour plots of maximum shear stress (left) and horizontal normal stress, S_{XX} (right). (t = 20 μs, σ_o = 25 MPa, V_{imp} = 10 m/s)

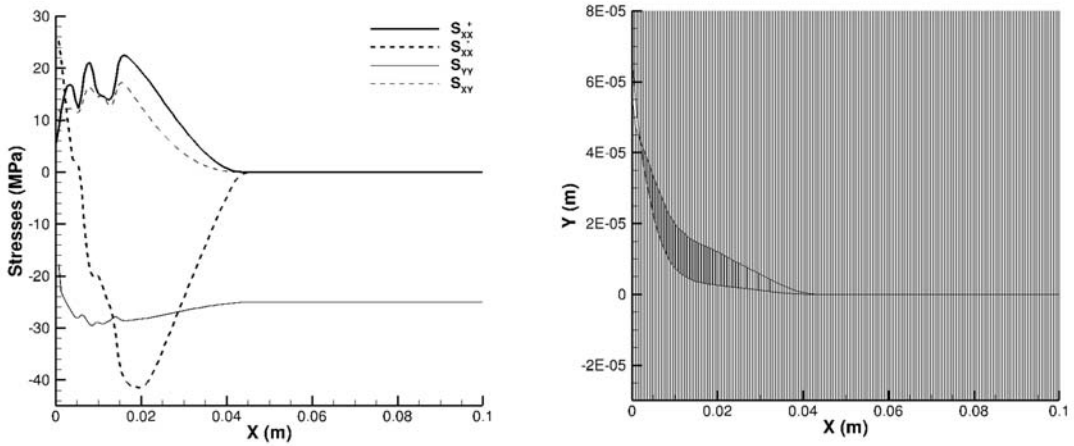

Figure 11. Plots of horizontal normal stress at the upper surface (S_{XX}^{+}), lower surface (S_{XX}^{-}), vertical normal stress (S_{YY}) and shear stress (S_{XY}) (left) and close-up of the mesh at the region of impact (right) (t = 20 μs, σ_o = 25 MPa, V_{imp} = 10 m/s)

4. Discussion

As compressive stress increases initiation of frictional sliding is delayed. For the three cases examined in this study sliding motion starts at 8 μs for crack-like mode, 12 μs for train of pulses mode and 15 μs for growing pulses mode. Hence the total slip in the interface is lower and behind for the case of growing pulses sliding mode, as is evident from Figure 12 (left). However Figure 12 (right) shows that when slip displacement is plotted at a constant time after initiation (in this case 6 μs after initiation) growing pulses mode is ahead of the others and total slip displacement is much higher compared to the other two modes. Note that the three sliding modes in Figure 12 are the same instances as the ones discussed so far.

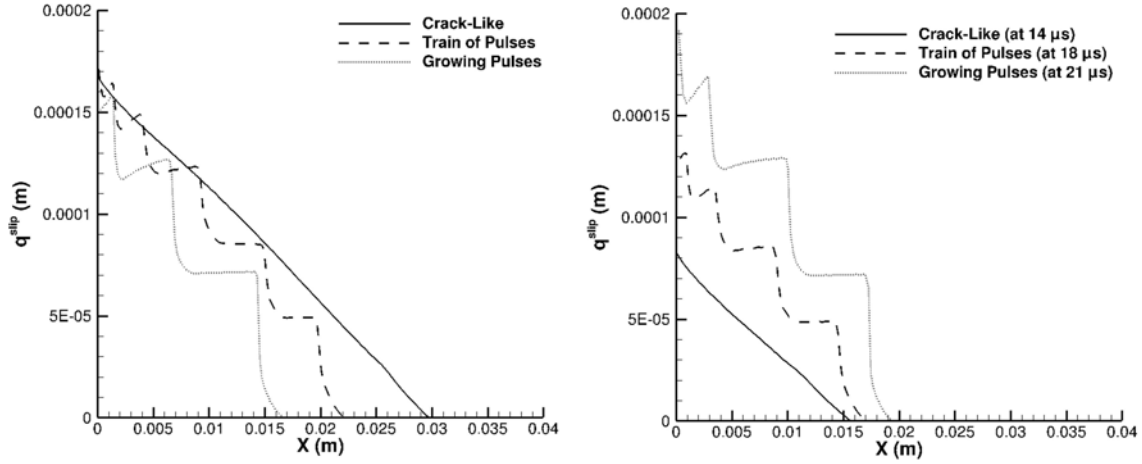

Figure 12. Total displacement in the three sliding modes 20 μs after the initiation of impact (left) and 6 μs after the initiation of sliding (right).

5. Conclusions

Dynamic frictional sliding modes between two plates under impact loading is numerically modeled using a rate- and state-dependent friction law. The three modes of sliding, expanding crack-like sliding, train of slip pulses, and solitary slip pulses are shown to exist depending on the impact speed and compressive load.

References

1. Heaton T.H., Evidence for and implications of self-healing pulses of slip in earthquake rupture, Physics of the Earth and Planetary Interiors, vol. 64, 1-20, 1990
2. Zheng G., Rice J.R., Conditions under which velocity-weakening friction allows a self-healing versus a cracklike mode of rupture, Bulletin of the Seismological Society of America, vol. 88, 1466-1483, 1998
3. Coker D., Lykotrafitis G., Needleman A., Rosakis A.J., Frictional sliding modes along an interface between identical elastic plates subject to shear impact loading, Journal of the Mechanics and Physics of Solids, vol. 53, 884-922, 2005.
4. Povirk G.L., Needleman A., Finite Element Simulations of Fiber Pull-Out, Journal of Engineering Materials and Technology, vol. 115, 286-291, 1993
5. Pierce D., Shih C.F., Needleman A., A tangent modulus method for rate dependent solids, Computers & Structures, vol. 18, 875-887, 1984